$3.00 PER COPY
$1.50 TO ASME MEMBERS

Tokamak Experimental Power Reactor*

W. M. STACEY, JR.

M. A. ABDOU
P. J. BERTONCINI
C. C. BOLTA
J. N. BROOKS
K. EVANS, JR.
J. A. FASOLO
J. C. JUNG
R. L. KUSTOM
V. A. MARONI
R. F. MATTAS

J. S. MOENICH
A. MORETTI
F. E. MILLS
B. MISRA
J. H. NOREM
J. S. PATTEN
W. F. PRAEG
P. SMELSER
D. L. SMITH
H. C. STEVENS
L. TURNER
S.-T. WANG
C. K. YOUNGDAHL

Mem. ASME

CTR Program,
Argonne National Lab.,
Argonne, Ill.

A conceptual design has been developed for a tokamak Experimental Power Reactor to operate at net electrical power conditions with a plant capacity factor of 50 percent for 10 years. The EPR operates in a pulsed mode at a frequency of ~ 1/min, with a ~ 75 percent duty cycle, is capable of producing ~ 72 MWe and requi es 42 MWe. The annual tritium consumption is 16 kg. The EPR vacuum chamber is 6.25 m in major radius and 2.4 m in minor radius, is constructed of 2-cm-thick stainless steel, and has 2-cm-thick detachable, beryllium-coated coolant panels mounted on the interior. A 0.28-m stainless-steel blanket and a shield ranging from 0.6 to 1.0 m surround the vacuum vessel. The coolant is H_2O. Sixteen niobium-titanium superconducting torodial field coils provide a field of 10 T at the coil and 4.47 at the plasma. Superconducting ohmic heating and equilibrium field coils provide 135 V-s to drive the plasma current. Plasma heating is accomplished by 12 neutral beam injectors which provide 60 MW. The energy transfer and storage system consists of a central superconducting storage ring, a homopolar energy storage unit, and a variety of inductor-convertors.

Tokamak Experimental Power Reactor

W. M. STACEY, JR.
M. A. ABDOU
P. J. BERTONCINI
C. C. BOLTA
J. N. BROOKS
K. EVANS, JR.

J. A. FASOLO
J. C. JUNG
R. L. KUSTOM
V. A. MARONI
R. F. MATTAS
J. S. MOENICH

A. MORETTI
F. E. MILLS
B. MISRA
J. H. NOREM
J. S. PATTEN
W. F. PRAEG

P. SMELSER
D. L. SMITH
H. C. STEVENS
L. TURNER
S.-T. WANG
C. K. YOUNGDAHL

ABSTRACT

A conceptual design has been developed for a tokamak Experimental Power Reactor to operate at net electrical power conditions with a plant capacity factor of 50% for 10 yr. The EPR operates in a pulsed mode at a frequency of $\sim 1/min$, with a $\sim 75\%$ duty cycle, is capable of producing ~ 72 MWe and requires 42 MWe. The annual tritium consumption is 16 kg.

The EPR vacuum chamber is 6.25 m in major radius and 2.4 m in minor radius, is constructed of 2 cm thick stainless steel, and has 2 cm thick detachable, beryllium-coated coolant panels mounted on the interior. A 0.28 m stainless steel blanket and a shield ranging from 0.6 to 1.0 m surround the vacuum vessel. The coolant is H_2O.

Sixteen niobium-titanium superconducting toroidal field coils provide a field of 10 T at the coil and 4.47 T at the plasma. Superconducting ohmic heating and equilibrium field coils provide 135 V-s to drive the plasma current. Plasma heating is accomplished by 12 neutral beam injectors which provide 60 MW. The energy transfer and storage system consists of a central superconducting storage ring, a homopolar energy storage unit, and a variety of inductor-convertors.

INTRODUCTION

An integrated conceptual design has been developed for a tokamak Experimental Power Reactor (EPR) (1). The design of the EPR was based upon technology that is consistent with a mid-to-late 1980s operation date. This paper summarizes the conceptual design, including the performance evaluation and cost estimate.

The design-basis performance objectives of the EPR are (1) to operate for 10 yr with a plant capacity factor of 50% [the plant capacity factor is defined as the product of the duty cycle (75%) and the plant availability (67%)]; and (2) to operate under conditions such that net electrical power production is feasible.

The principal geometric parameters of the EPR are given in Table 1 and in the vertical section view shown in Fig. 1. A detailed vertical section view is shown in Fig. 2, and a plan view is shown in Fig. 3.

PLASMA PHYSICS AND PERFORMANCE ANALYSIS

Steady-state plasma parameters corresponding to the reference design are given in Table 2. A wide

Table 1   EPR Geometrical Parameters

Radius (m)	
Major, R_0	6.25
Plasma, a	2.1
First-wall, r_w	2.4
Aspect ratio, $A = R/a$	2.98
Plasma volume (m^3)	544
Toroidal vacuum chamber volume (m^3)	711
First wall area (m^2)	592
Blanket thickness (m)	
Inside	0.58
Outside	0.97
Toroidal field coils	
No.	16
Horizontal bore, R_{bore} (m)	7.78
Vertical bore, Z_{eff} (m)	12.6

Table 2   Steady-State Plasma Parameters
— Reference Design

|		
Poloidal beta, β_p	1.7	
Total beta, β_t	0.048	
Safety factor		
Magnetic axis, q(0)	1.00	
Plasma surface, q(a)	3.05	
Plasma radius, a (m)	2.1	
Aspect ratio, A	2.98	
Average temperature, $\bar{T}$ (keV)	10	
Effective ion charge, Z_{eff}	1.3	
Confinement for ignition, $n\tau_E$ (s/m^3)	2.4×10^{20}	
Peak field at TF coils, B_{max}^{TFC} (T)	10.0	8.0
Field at centerline, B_{t0} (T)	4.47	3.58
Plasma current, I_p (MA)	7.58	6.06
Average D-T ion density, $\bar{n}_{DT}$ (m^{-3})	9.4×10^{19}	6.0×10^{19}
Power output, P_T (MW)	638	261
Neutron wall load, P_w	0.86	0.35
Ratio of $n\tau_E$ required for ignition to TIM value of $n\tau_E$, α_{TIM}	1.0	4.0
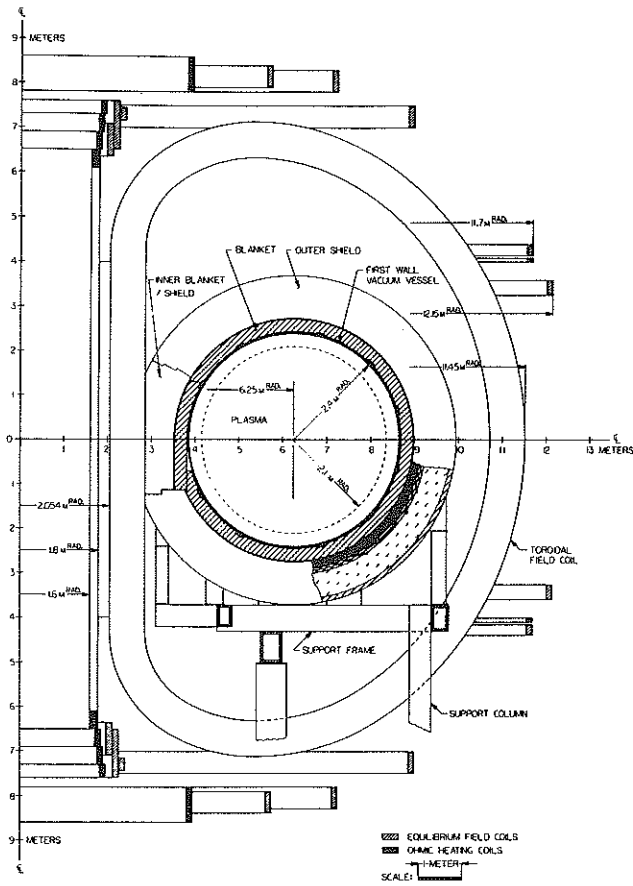
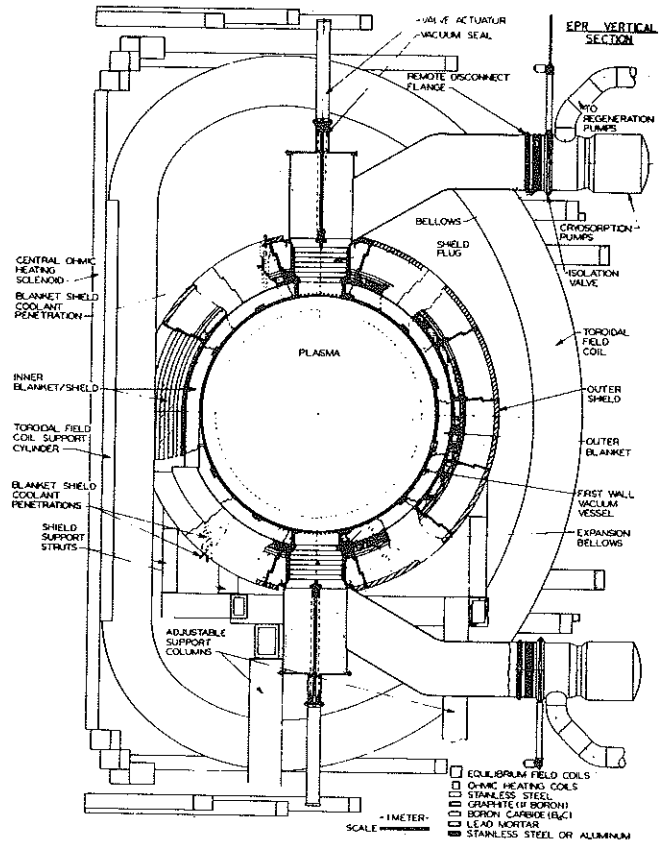Fig 1 EPR vertical section dimensions
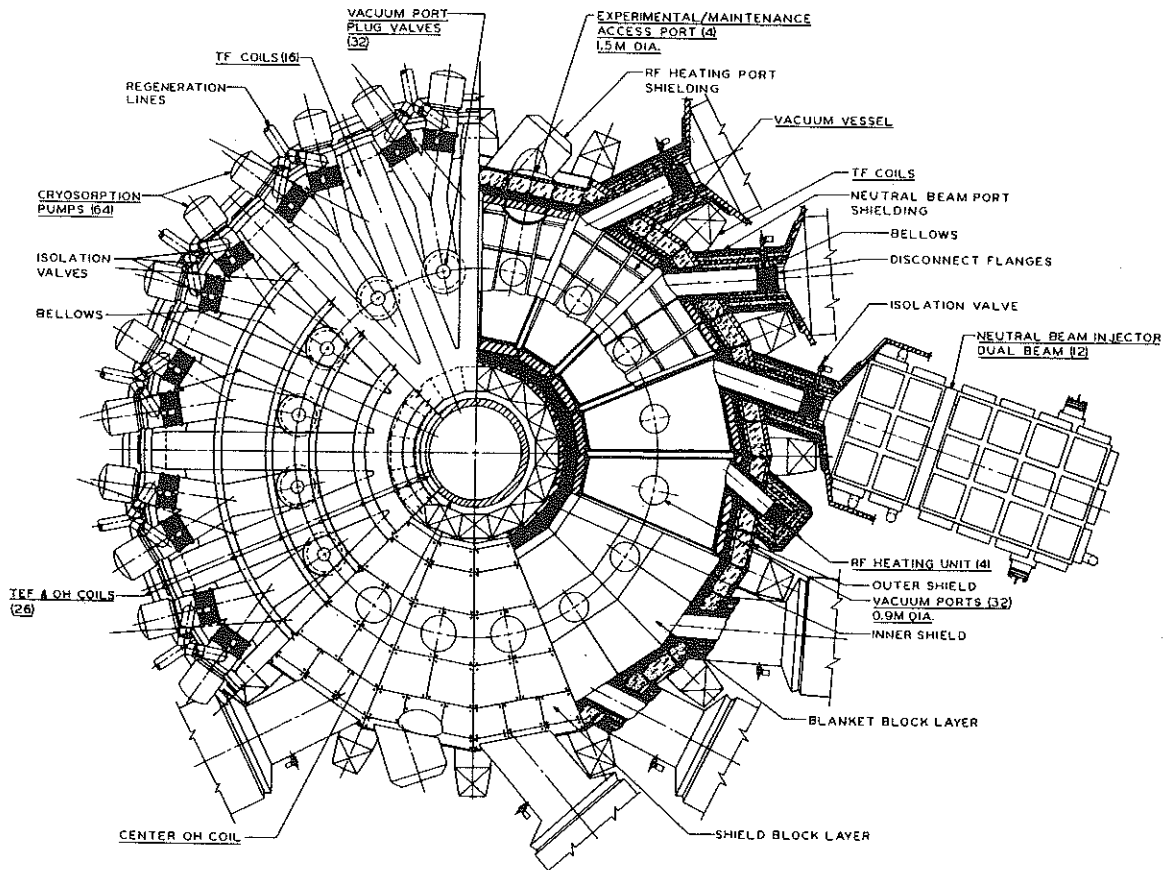
Fig. 2 Detail of vertical section of EPR

Fig. 3 ANL experimental power reactor plan view

range of performance parameters is possible, corresponding to a range of possible MHD equilibria and to a range of possible operating temperatures and values of energy confinement. Extensive analyses were performed to insure that the parameters shown in Table 2 are representative of the range of plasma conditions that may be obtained in EPR. With supplemental beam heating, the power output is not jeopardized by the possibility of subignition energy confinement.

Requirements on the plasma driving and heating systems and the power performance characteristics are determined from burn cycle dynamics simulations of the plasma, the ohmic-heating (OH) and equilibrium-field (EF) coil systems, and the neutral-beam injection system. The basic burn cycle is depicted schematically in Fig. 4, where the times correspond to the reference burn cycle. The plasma conditions of the reference case at $B_{max}^{TFC} = 10$ T (see Table 2) are approximated during the burn (flat-top) phase, and the dynamics calculations are constrained by the limit $\beta_p \leq \beta_p^{max} = 1.71$.

A variety of startup procedures were simulated in order to determine a compromise among several conflicting economical and technological limitations. The critical parameters which, to some extent, can be traded off against each other are (1) energy transfer from the homopolar OH supply (U_{OH}); (2) peak power required from the EF supply (P_{EF}); (3) total energy drawn from the energy storage unit for beam heating (U_{BE}); (4) maximum rate of change of the field in the OH coil ($\dot{B}_{OH}$). Initiation of beam heating midway through the OH current reversal, thereby reducing

resistive losses during startup, was found to be beneficial. The time of the OH current reversal, Δt_{OH}, is an important factor in determining the requirements of the plasma driving and heating systems, as indicated in Fig. 5. On the basis of these results, $\Delta t_{OH} = 2$ s was chosen for the reference case. As a result of extensive studies of this type, the maximum requirements shown in Table 3 were identified.

Table 3   Plasma Driving and Heating System Maximum Requirements

Ohmic heating coil system	
Volt-seconds to plasma	85
Peak field, B_{OH} (T)	5.0
Maximum field rise, $\dot{B}_{OH}$ (T/s)	6.7
Maximum voltage, V_{OH} (kV)	51
Maximum current, I_{OH} (kA)	80
Maximum power required, P_{OH} (MW)	1900
Maximum energy transfered, U_{OH} (MJ)	1200
Minimum current reversal time, Δt_{OH} (s)	2
Equilibrium field coil system	
Volt-seconds to plasma	50
Maximum voltage, V_{EF} (kV)	21
Maximum current, I_{EF} (kA)	80
Maximum power required, P_{EF} (MW)	420
Maximum energy transfered, U_{EF} (MJ)	1500
Neutral beam injection system	
Deuteron energy (keV)	180
Power to plasma, P_B (MW)	60
Energy to plasma, U_B (MJ)	300
Energy from energy storage, U_{BE} (MJ)	1000

Fig. 4   Burn cycle scenario

4

P (GW)   U (GJ) $\dot{B}$ (T/s)   B (T)

0.6 — 1.2 — 12 — 6

0.5 — 1.0 — 10 — 5

0.4 — 0.8 — 8 — 4

0.3 — 0.6 — 6 — 3

0.2 — 0.4 — 4 — 2

0.1 — 0.2 — 2 — 1

0 — 0 — 0 — 0

CASE 4   5   6

1.0   2.0   4.0

OH Reversal Time Δt_{OH}, s
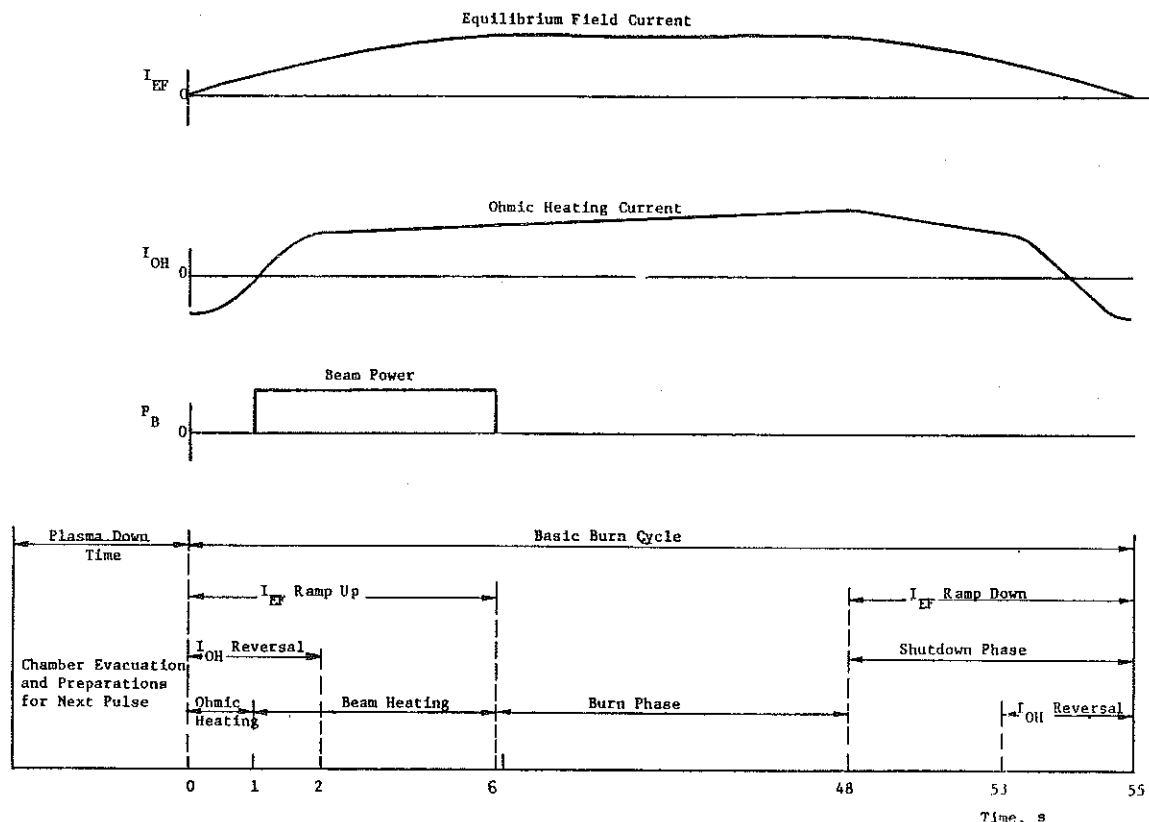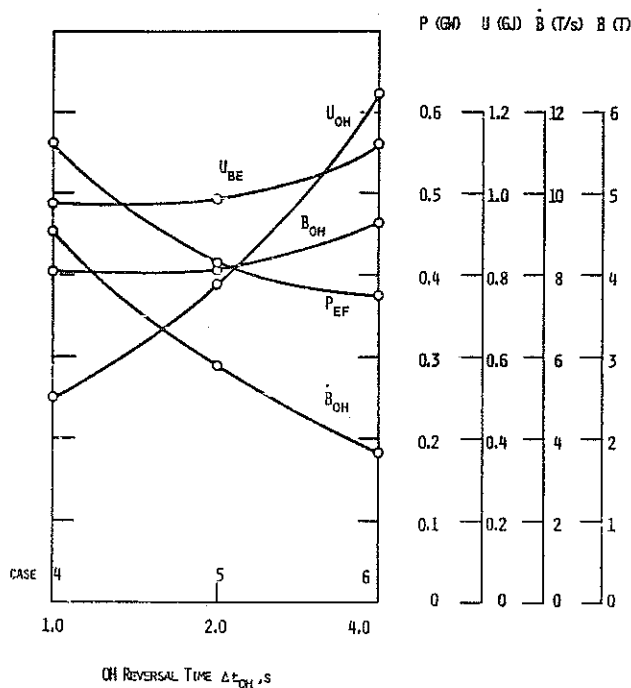
Fig. 5   Effect of OH current reversal time on
plasma driving and heating system requirements

The net energy flow for a burn cycle is shown
schematically in Fig. 6. A total of 16.34 GJ of energy
is incident on the first wall; of this, 15.96 GJ is
produced by fusion and 0.38 GJ results from beam and
ohmic heating of the plasma. An additional 0.45 GJ of
thermal energy is recovered from the beam injector sys-
tem, so that 16.79 GJ of thermal energy is available
for conversion to electricity. With a conversion effi-
ciency η_T = 30%, this would result in 5.04 GJ of elec-
trical energy. Deducting the 2.95 GJ of electrical
energy required to run the plant — 1.51 GJ to run the
auxiliary systems and 1.44 GJ to make up deficits in
the energy storage system caused by energy losses in
the injection (0.98 GJ) and OH/EF (0.46 GJ) systems —
results in 2.09 GJ net electrical energy. Averaging
this over a 70 s operating cycle (a 55 s burn plus a
15 s replenishment period) results in a net electrical
power of 29.9 MW. The EPR may well operate without a
thermal conversion system, in which case 2.95 GJ per
cycle, or a continuous power of 42.1 MW, is required
from the electric power grid.

MAGNET SYSTEM

The EPR magnet system consists of the toroidal-
field (TF) coil system and the poloidal-field coil
system. These coils interact with one another during
operation and also interact with the other systems of
the EPR. The magnet system design was developed in
sufficient detail to evaluate problems in the construc-
tion and operation of EPR magnets.

Toroidal Field Coils

The TF coils use niobium-titanium as the supercon-
tor because of its good ductility and proven perfor-
mance in large magnets. The toroidal field strength
should be as high as practical in order to enhance the
plasma confinement and boost the power performance. A
peak field of 10 T can be achieved with a large amount
of superconductor at 4.2°K or with much less supercon-
ductor at 3°K. It is more economical to operate the

10-T TF coil at 3°K because the difference in refrig-
eration cost is much smaller than the difference in the
cost of the superconductor. The problem of refrigera-
tion at temperatures lower than 4.2°K for large systems
was evaluated. The TF coils will achieve 10 T peak
field at 3°K and 8 T peak field at 4.2°K with about
0.5°K temperature allowance for each case; 8 T is the
minimum goal and 10 T is the maximum goal in the TF
coil design.

A TF coil system consisting of 16 pure-tension
"D"-shape coils with a horizontal bore of 7.78 m pro-
vides adequate space for the vacuum chamber, blanket
and shield, provides adequate access for assembly and
repair, and has a satisfactorily small maximum field
ripple of 1.3%. The TF coil system is summarized in
Table 4.

The superimposing field on the TF coils from the
poloidal coils was found to be the most troublesome
factor in the TF coil design. The out-of-plane load
is large and creates serious problems for the struc-
tural design as well as a threat to the coil stability
from bending moments and shear stresses in the coil
structure. Moreover, unacceptably large ac losses will
occur in the TF coil unless either the conductor is
made of cable or the coil is shielded against changing
fields. Both of these possibilities were evaluated.

The sponginess of cable conductor threatens coil
structure integrity. In addition, cabling the conduc-
tor does not overcome all ac losses; changing the
parallel field still couples filaments in a single
strand. These ac losses, proportional to the conduc-
tor length, are still unacceptably large and the con-
ductor stability is very poor. One possible solution
is periodic twist-pitch reversal, but this is as yet
only a hypothesis.

For the EPR, the option of a field shield was
chosen. It was found that an aluminum shield operating
at a mean temperature of 18°K is a reliable means of
overcoming the varying field superimposed by the poloi-
dal field coils. Detailed analyses of ac loss in field
shields, the out-of-plane load, and dc field soaking
were completed. AC losses in the shield are preferable
to ac losses in the conductor. Superconducting shields
were also considered, but were not adopted because
their use would require considerable development work.

With the coils shielded, a more solid cable con-
ductor can be used. A conductor 0.5 cm thick and 30
to 50 cm wide has been chosen as the reference conduc-
tor. It will carry a current of 60 kA. Each TF coil
will consist of two jelly-rolled windings side by side
with a central rib between them. The combination of
the central rib and the flat conductor with one turn
per layer makes a strong structure with good transfer
for hoop stress and centering force, a good mechanical
stability, good rigidity against out-of-plane loads,
and assurance of cryostatic stability for the TF coils.

Coil protection is also facilitated by this con-
ductor design with a high current and relatively few
turns. During a rapid (8-1/2 min) discharge, the
voltage between neighboring turns will be low; and
even the maximum voltage with respect to ground can be
limited to 2000 V.

The TF coils must be operated in series at all
times; otherwise unequal currents in different coils
could create large forces and torques between coils
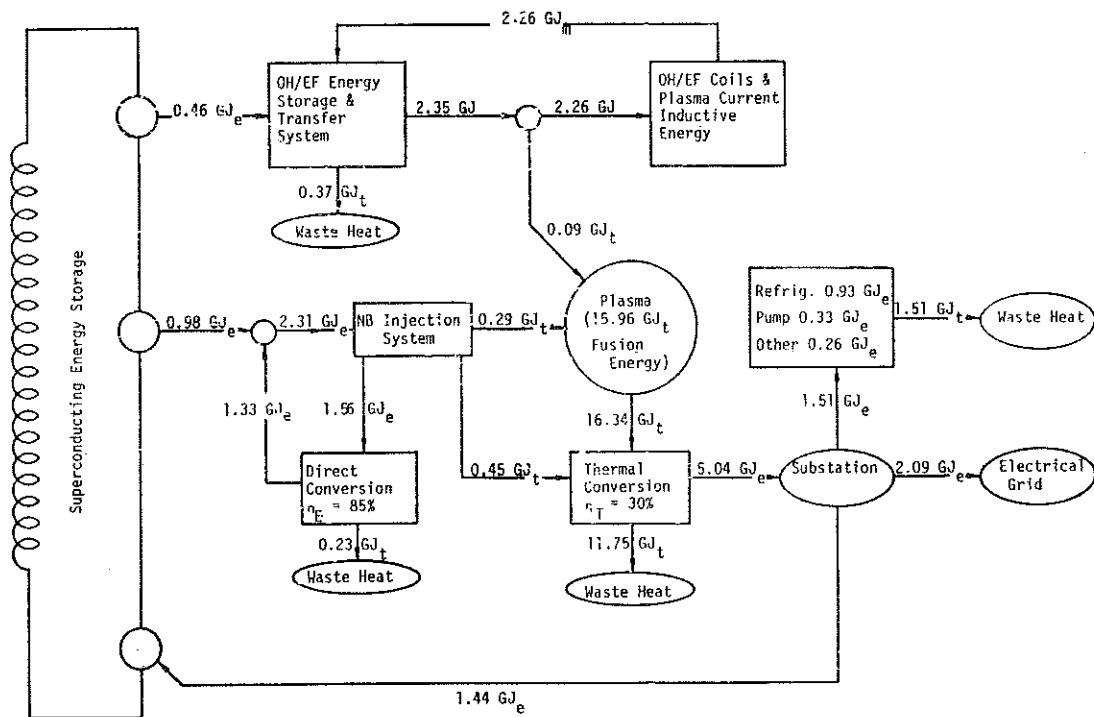and large bending moments in each TF coil, even if the

Superconducting Energy Storage

2.26 GJ$_m$

0.46 GJ$_e$ → OH/EF Energy Storage & Transfer System — 2.35 GJ → 2.26 GJ → OH/EF Coils & Plasma Current Inductive Energy

0.37 GJ$_t$ → Waste Heat

0.09 GJ$_t$

0.98 GJ$_e$ → 2.31 GJ$_e$ → NB Injection System → 0.29 GJ$_t$ → Plasma (15.96 GJ$_t$ Fusion Energy)

Refrig. 0.93 GJ$_e$ / Pump 0.33 GJ$_e$ / Other 0.26 GJ$_e$ → 1.51 GJ$_t$ → Waste Heat

1.33 GJ$_e$ 1.56 GJ$_e$

16.34 GJ$_t$

1.51 GJ$_e$

Direct Conversion η_E = 85%

0.45 GJ$_t$ → Thermal Conversion η_T = 30% → 5.04 GJ$_e$ → Substation → 2.09 GJ$_e$ → Electrical Grid

0.23 GJ$_t$ → Waste Heat

11.75 GJ$_t$ → Waste Heat

1.44 GJ$_e$

Fig. 6   Net energy flow in reference burn cycle (with thermal energy conversion)

Table 4   Toroidal Field Coil System

Superconductor/stabilizer/ insulator/support	Nb–Ti/Cu/ fiberglass epoxy/SS	Ampere-turns (MAT) Total Coil	134 8.37
No. of coils	16	Turns/coil	70 × 2
Coil shape	pure tension R_{10} = 2.45 m R_{20} = 11.1 m	Mean turn length (m)	36
		Total conductor length/coil (A–m)	151.2 × 10^6
Field ripple (%)	1.3	Coil weight/coil (Ton)	∿208
Maximum access (m)	∿3	Coil and bobbin cross section (m^2)	0.619
Peak field (T)	10 @ 3°K 8 @ 4.2°K	Bobbin Material Thickness (cm)	316 SS 1.25
Bore (m) Vertical Horizontal	12.6 7.78	Winding cross section (m^2)	0.572
Field in plasma, B_t (T) 10 T peak field 8 T peak field	4.32 3.46	Average current density (A/cm^2) Over bobbin and coil Over coil winding Over copper	1352 1463 3660
Stability	cryostatic	Smallest radius of curvature at ∿10 T field region (m)	1.98
Temperature allowance (°K)	0.5	Average hoop force-turn (1b)	133 × 10^3
Conductor design	monolithic	Average turn cross section (cm^2)	40.6
Cooling	pool boiling	Cross section ratio, SS/Cu	∿1.5
Operational current (kA/turn)	60	Overall average stress (psi) Stainless steel Copper	26,000 14,500
Stored energy (GJ) Total Coil	30 1.875	Length of straight segment (m)	8.56
Inductance (H) Total Coil	16.7 1.04	Compressive pressure (psi)	7660
		Circumferential stress (psi)	<74,000
		Refrigeration power (MW)	14.3

TF coil is in pure-tension shape. These would produce catastrophic damage to the TF coil system.

The radiation shield is designed to protect the TF coils from nuclear heating and radiation damage. The nuclear heat load is 1.5 kW, which is negligible in comparison with other heat dissipation in the TF coils. The copper stabilizer is designed to tolerate a radiation-induced resistivity of 1.5×10^{-8} Ω-cm. The shield is designed so that this value occurs after 2.5 MW-yr/m^2 integrated first-wall neutron load, which corresponds to 10 yr of operation at the nominal wall load of 0.5 MW/m^2 and a 50% capacity factor. The dose of 3.5×10^8 rads to the epoxy insulator is well below the range 10^9-10^{10} rads at which its properties degrade.

Poloidal Field Coils

The poloidal field coils present problems different from those of the TF coils, but equally challenging. The poloidal field coils consist of the initiation-trimming (IT) coils, the ohmic heating (OH) coils, and the equilibrium field (EF) coils. The OH coils and the EF coils are superconducting and are located outside the TF coils, as shown in Fig. 1. The smaller IT coil system is made of water-cooled copper and is located near the first wall. The IT coils initiate plasma discharge by delivering 4 V-s in 10 ms. The field from the IT coils can also be used to trim the plasma position.

Although the OH coils serve as the transformer primary for producing the plasma current and the EF coils provide equilibrium for the plasma, both coil systems have nearly identical problems, e.g. large stored energy, high operational current, rapid charging and discharging, and ring coil configuration. For this reason, the conceptual design of the eight pairs of EF coils and six pairs of OH coils were carried out together.

The design requirements summarized in Table 3 for the OH and EF coil systems were specified as a result of a detailed trade-off study. Burn cycle dynamic simulations of the plasma, the coupled OH and EF systems and the plasma heating systems were performed. Free-boundary plasma MHD equilibrium calculations were utilized in the design of an equilibrium field that would produce the circular plasma.

Characteristics of the OH and EF coils are given in Table 5. The OH coils and EF coils both have a maximum operational current of 80 kA supplied by two parallel 40 kA cables with fully transposed strands. The OH coils have 837 turns in each parallel path; the EF coils have 464. The charging voltage for the OH coils is 48 kV and the turn-to-turn voltage is about 60 V. The charging voltage for the EF coils is 21 kV and the turn-to-turn voltage is about 50 V. In the helium gas environment, the minimum turn-to-turn separation must be about 0.3 mm.

Multilayer coils would require large gaps between layers and present an awkward problem for coil design, especially for the long OH solenoids. Therefore, each coil will be wound with a single-layer conductor 15 cm wide.

The EF coils and OH coils will be cooled by helium pool boiling at 4.2°K, 1 atm pressure. Pool boiling is simple, inexpensive, reliable, and easy to control. Above all, a rather small heat transfer flux is ade-quate to remove the conductor ac losses if the helium bubbles can be properly vented to avoid bubble accumulation within the winding. Under this circumstance, the heat transfer flux ceases to be an important factor in determining the coil stability; instead the coil stability depends on the conductor current density, the amount of liquid helium surrounding the conductor, and the extent of coil disturbances.

The equilibrium field must penetrate the blanket and shield to act on the plasma, but the blanket and shield are about a meter thick and consist mostly of metal such as stainless steel. Eddy currents in this material would distort the equilibrium field and delay its penetration if the blanket and shield were not sufficiently segmented. For a blanket and shield design of 16 segments, each made of 43 blocks, field distortion or time delay will be reduced to an insignificant level.

Structural Support

Two structural support concepts, a torque shell and a torque frame, were developed.[1] The torque shell design uses shear webs located between the TF coil cryostats to provide continuous support for the coil and to cancel the induced torques. This design provides the lightest weight design but requires removal of the shear web panels to permit access to the blanket and shield. The torque frame concept uses a frame at the top and bottom of the reactor to transfer the TF coil loads to the reactor building wall and floor, respectively. Both concepts provide blanket and shield access through an ∿3 × 8 m opening between TF coils. Very little access, if any, will be available from above and below the TF coil because of required structure. Openings for vacuum ducts and instrumentation, however, can be provided through this structure. The floor area around the reactor will not be restricted by structural members with either concept, thereby providing for ease of locating components such as neutral beam injectors and for freedom of movement for maintenance equipment. The outer and upper poloidal coils can be removed using their supporting structure as a lifting fixture, and the combined weight is compatible with planned crane capacity. The lower poloidal coils are captivated by the various support columns and require an in-place repair/replacement facility, which was conceptually included in the design. Use of 7075-T6 aluminum alloy joined by bolting results in a substantially lighter and lower cost structural support design than can be achieved using welded stainless steel. The torque shell concept has been tentatively chosen as the reference option.

PLASMA HEATING

Supplemental heating, in addition to ohmic heating, is required to heat the EPR plasma to ignition temperatures. A power input to the plasma of 60 MW is needed for about 5 s during startup, and somewhat less power may be required for periods up to a minute to maintain the burn in the face of unfavorable plasma conditions. Current experience dictates that neutral beam heating be the reference option for this supplement. Radio-frequency heating is considered as the primary backup option.

---

[1]
This work was performed by McDonnell-Douglas Astronautics Company-East in collaboration with ANL.

Table 5 OHC/EFC Magnet Characteristics

	OHC	EFC
Superconductor/stabilizer	Nb–Ti/Cu	
Coil design	Single layer	
Conductor design	Fully transposed cable	
Stablity	Cryostatic	
Cooling	Pool boiling	
Operating temperature (°K)	4.2	
Average current density (A/cm^2)	2640	2946
Magnetic field (T)		
in flux core	~5	
at plasma center		~0.46
Ampere-turns (MAT)	67	±18.6
Total conductor length (MA meters)	847	996
Maximum dB/dt in conductor (T/s)	6.7	~1
Stored energy in OH/EF/plasma field (MJ)	2262	
Maximum operational current (kA)	80	80
No. of turns	837	464
Self inductance (H)	0.48	0.52
Mutual coupling	$K_{OHEF} = 0.015$	
Power supply voltage (kV)	48	21
Volt-seconds to plasma (V-s)	85	50
Coupling coefficient to plasma ring	$K_{OHP} = -0.2422$	$K_{EFP} = -0.2566$

Table 6 Neutral Beam Injection System Characteristics

	(Reference) Design 1	Design 2	Design 3a	Design 3b
Atomic ion	D^+	D^+	D^-	D^-
Target for $D^\pm \to D^0$	D_2 gas	D_2 gas	D_2 gas	Li plasma
Beam composition (D^+, D_2^+, D_3^+/D^-)	(0.75,0.18,0.07/-)	(0.95,0.03,0.02/-)	(-/0.95)	(-/0.95)
Neutral beam power (MW)	60	60	60	60
Neutral beam energy (keV)	180	180	180	180
Neutral beam current (Equiv. A)	333	333	333	333
No. of injectors	12	12	6	6
No. of ion sources/injector	2	2	2	2
Type of grid	multiaperture	multiaperture	multiaperture	multiaperture
Ion beam current density (A/cm^2)	0.135	0.175	0.135	0.135
Ion beam power (MW)	441	338	113	81
Gas load/injector (Torr-ℓ)	110	57	41	11
Direct conversion efficiency	0.85	0.85	0.85	0.85
Thermal conversion efficiency	0.30	0.30	0.30	0.30
Electrical power efficiency	0.29	0.41	0.66	0.77
Overall power efficiency	0.34	0.45	0.66	0.77
Net power input. (MW)	207	145	91	78

Neutral Beam Injection

Three neutral beam injection systems have been designed. These are summarized in Table 6. The reference design is based on modest extrapolations beyond presently achieved results with D^+ sources. The second design is based upon improved D^+ sources. The third design, which would require considerable advances in source technology, is based upon direct-extraction D^- sources, with neutralization by a gas target (3a) or by a lithium plasma (3b). All designs employ energy recovery, and the first two designs inject only the $D^+ \rightarrow D^0$ component into the plasma.

In the reference design, 12 injectors, arranged as shown in Fig. 3 to tangentially inject into the plasma in a symmetrical clockwise and counter-clockwise pattern, provide 60 MW of 180 keV deuteron beams to the plasma. Each injector has two ion sources. The beam line for each ion source includes an accelerator to increase the energy of the D^+ ions, a magnet separator and energy grid to remove molecular ions and directly convert their energy into electricity, a neutralizer to form the neutrals, and a thermal energy recovery system. The pair of beams in each injector travel ~4 m along a beam duct and pass through a 0.75 m diameter port in the toroidal vacuum chamber wall. An electrical power efficiency (neglecting thermal energy recovery) of 0.29 and an overall power efficiency (including thermal energy recovery) of 0.34 are achieved with the reference design. These power efficiencies decrease rapidly with beam energy, because of a decrease in the neutralization efficiency in D_2 gas.

Substantial improvements in power efficiency and corresponding reductions in power requirements and gas loads can be realized if D^+ ion sources are developed with a very high atomic ion component, as indicated by Design 2 in Table 6. Even more dramatic improvements could be realized if direct-extraction D^- sources are developed.

Radio-Frequency Heating

Radio-frequency (rf) wave heating is an attractive alternative to neutral beam heating, from the technological point of view, since efficient power sources exist for several heating modes and the neutron penetration problems intrinsic to the neutral beam injectors can be ameliorated. However, wave heating experiments have not encountered the same degree of success as neutral beam experiments in heating plasmas.

Two rf heating designs were developed, one based upon heating in the lower hybrid resonance (LHRH) and the other in the ion cyclotron resonance (ICRH). The EPR reference design has four rf heating stations supplying 20 MW to the plasma, for added heating capability and experimentation. If rf heating becomes the primary option, the EPR design can accommodate 16 rf stations by replacing the neutral beam injectors with rf systems. The characteristics of ICRH and LHRH systems which could provide 25 and 60 MW of heating power to the plasma are shown in Table 7.

ENERGY STORAGE AND TRANSFER SYSTEM

The energy storage and transfer (EST) system for the EPR consists of a central energy storage inductor (ESI), rectifiers to transfer energy between the ESI and the OH, EF, and neutral beam systems and a rectifier to transfer energy from the substation into the ESI. A separate inertial energy storage unit, consisting of radially stacked homopolar generators, is incorporated in the OH system, so that the inductive energy in the OH system is essentially transferred between the OH coils and inertial storage inductor, with the central ESI providing makeup for losses. Inductive energy is transferred between the OH/EF coils and the plasma current, with some dissipative loss in the plasma. The neutral beam energy is deposited in the plasma or dissipated in the injection system. Electrical energy is recovered directly and recirculated in the neutral beam injection system. If rf plasma heating is used instead of neutral beam injection heating, the required energy is transferred from the ESI by a rectifier. The EST system is depicted schematically in Fig. 7 and summarized in Table 8.

The OH coil current is reversed at the start and end of the burn cycle. The OH coil energy storage unit is designed to transfer and store the bulk of the OH coil stored energy during the reversal periods by using radially stacked drum-type homopolar generators. Additional energy required to provide 5 V-s for resistive plasma losses is transferred into and out of the OH coil during the burn cycle using an SCR-type inductor-converter bridge as the major transfer mechanism between the OH coil and a central superconducting energy storage inductor. The central ESI makes up the 0.46 GJ of energy which is dissipated in the OH-plasma system each burn cycle.

The design of the homopolar generators is based on radially stacked epoxy fiberglass insulating cylinders and Type 17-4 stainless steel cylinders. The insulated cylinders are rigidly supported and aligned with respect to the central axis. The conducting cylinders rotate independently on a type of air bearing designed into the insulating cylinders. The innermost and outer-most cylinders are made of insulating materials, so that high voltages can be achieved by electrically connecting many generators in series. A radially directed, azimuthally uniform magnetic field of about 5 T is produced by niobium-titanium superconducting coils. Brushes are located along the edges of the cylinders and connected so that current flows back and forth in the axial direction. Adjacent cylinders counter rotate. The arrangement is called the counter cyclonic generator (CCG).

The energy transfer system for the EF coils must be actively controlled because the power demand varies with plasma current and temperature. The design of the power supply is based on storing and transferring the energy between the EF coils and the superconducting energy storage inductor using an inductor-converter (I-C) capacitor bridge. The design of the EF coil power supply uses typical SCR units currently available on the market. A three-phase bridge is used with 35 mF, 10 kV capacitors in each phase.

The design of the neutral beam injector energy transfer system is composed of two major components; a saturated time-delay transformer (STDT), which uses the saturation effects of magnetic cores to act as a current surge limiter, and a high-frequency, polyphase-controlled rectifier using SCR switches to enable rapid de-energization of the beam in periods of less than 100 µs. The beam heating pulse is designed to last for 5 s. Energy is added to the central ESI throughout the fusion reactor cycle. The injector power supply extracts energy directly from the ESI during the beam heating phase, so that the power grid never sees a power bump. An I-C drives a high-fre-

9

Table 7   RF Heating Parameters

	ICRH	LHRH
Pump frequency (MHz)		
8 T	54.0	1120
10 T	68.6	1190
Output power (MW)		
4 ports	25	25
10 ports	60	60
Transmission efficiency from source to port (%)	64	48
Pulse duration, heating (s)		
25 MW	12.9	12.9
60 MW	5.4	5.4
Duty cycle (%)		
25 MW	17.2	17.2
60 MW	7.2	7.2
Launcher	1/4 turn loops	"Grill" waveguide 8 across × 2 high
Transmission scheme	Coaxial cables	Waveguides
High power source	Tetrode amplifier	Klystron

Table 9   Vacuum System Parameters

	Toroidal	Neutral Beam
Volume	754 m^3	250 m^3/injector
Surface area	771 m^2	254 m^2/injector
Gas load	2588 Torr-ℓ	110 Torr-ℓ/s per injector
Cryosorption pumping	32 – 25000 ℓ/s pumps	100 m^2 panel/injector
Effective pumping speed	4.25×10^5 ℓ/s	5×10^6 ℓ/s per injector
Secondary pumps		
Al/Zr getter pumps	32 – 10000 ℓ/s	12 – 25000 ℓ/s
No. 1300 CFM blower stations	16	Use same pumps
No. 1400 ℓ/s turbomolecular pumps	16	Use same pumps

Table 8   Energy Transfer and Storage Systems -- Maximum Ratings

```
Ohmic Heating Systems

    Drum homopolar generators
        No. of generators in series        16
        No. of drums/generator              6
        Total energy transfer (MJ)       1200
        Peak power (MW)                  1900
        Peak voltage (kV)                  51
        Peak current (kA)                  68
        Equivalent capacitance (F)        0.897

    Rectifier system
        Type                             Inductor-converter bridge
        Energy transfer (MJ)              600
        Peak power (MW)                    66
        Peak current (kA)                  80
        Peak voltage (kV)                 0.8

Equilibrium Field System

    Type                                 Inductor-converter bridge
    Energy transfer (MJ)                 1500
    Peak power (MW)                       416
    Peak current (kA)                      80
    Peak voltage (kV)                      21
    Peak switching frequency (Hz)        1330
```

Neutral Beam System[a,b] (60 MW)

```
    Type                                 SCR, DC/AC/DC at 10 kHz
    Energy transfer (GJ)                  1
    Voltage (kV)                         180
    Power (MW)                           207
```

RF System (60 MW)[b]

```
    Type                                 5 phase inductor-converter bridge
    Voltage (kV)
        ICR                              18.0
        LHR                              64.5
    Power (MW)
        ICR                               94
        LHR                              125

Central Energy Storage Inductor

    Type                                 Superconductive ring dipole inductor
    Energy stored (GJ)                   3.2
    Energy transfer (GJ)                 2.4
    Peak current (kA)                     80
    Peak power (MW)                      620
    Average power from 60 Hz line (MW)    21
```

[a]Assumes electrical energy recovery in power supply.
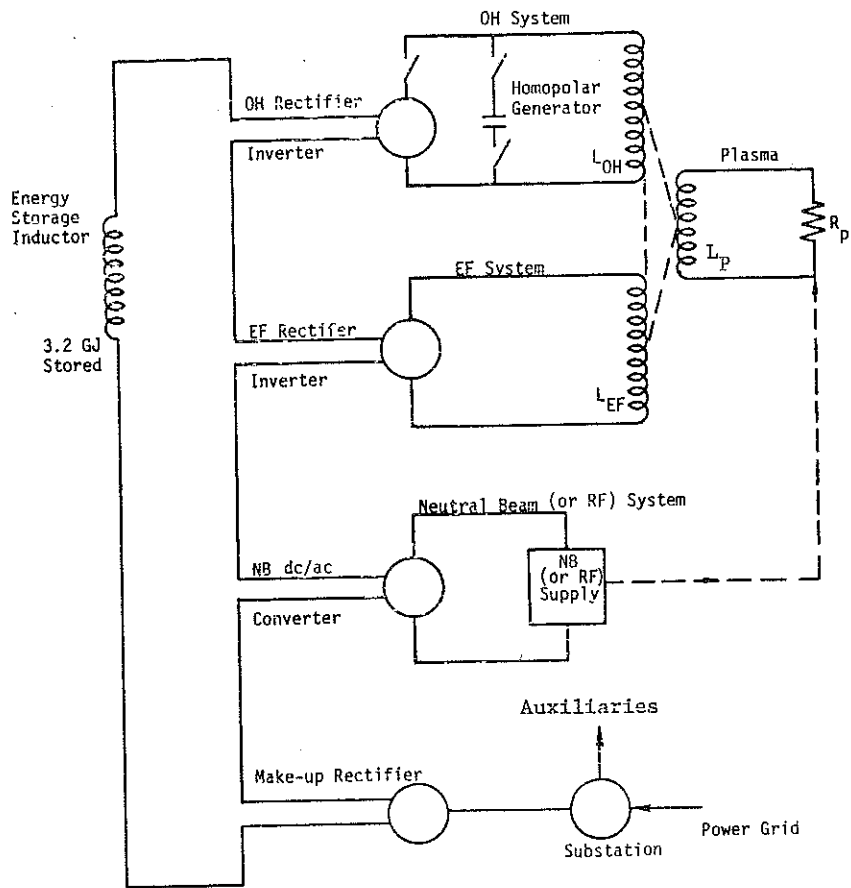
[b]Neutral beam and rf are alternative options.

Fig. 7   Circuit diagram

quency polyphase inverter. A 10 kHz voltage is developed in a summing transformer, filtered and subsequently rectified. The output lead is connected to the injector through an STDT. A coil on the STDT is connected to a controlled time delay circuit that will trigger a crowbar and interrupting switches in the event the primary neutral beam injector protection systems fail.

The power supplies for the ion cyclotron region and the lower hybrid region rf heating systems are designed using the I-C concept used for the EF coil. Five-phase I-C bridge networks are designed to transfer energy from the ESI to the rf conversion units. Five-phase networks are used to avoid objectionably large voltage fluctuations on the frequency conversion tubes.

In order to operate the poloidal coil, neutral beam and rf systems, it will be necessary to store energy on site so that large power pulses required to initiate and terminate the tokamak discharge do not perturb the electrical power network. A superconductive energy storage inductor was designed to handle these energy pulses. The energy storage ring uses 21.4 MW at a constant input rate and provides a peak net withdrawal of 2.4 GJ at the end of beam heating. The maximum current is 80 kA at a maximum short time-averaged voltage of 15 kV. The ring has a major radius of 5.7 m and a minor radius of 0.8 m. The coil will use 0.58 m^3 of niobium-titanium and is constructed of pancakes separated by micarta or fiberglass-epoxy boards. Alternate pancakes are wound clockwise and counterclockwise to facilitate layer-to-layer connections. Conductor transposition is achieved by winding top and bottom halves with 40 kA cable and operating coil halves in parallel. There are a total of 12 layers of coil.

VACUUM SYSTEMS

The EPR toroidal vacuum system must: (1) reduce the residual gas pressure in the toroidal chamber from $\sim 2 \times 10^{-3}$ to $\sim 1 \times 10^{-5}$ Torr in ~ 15 s after the burn pulse; and (2) achieve a base pressure of less than 10^{-8} Torr at the beginning of an operational period. These criteria can be satisfied by thirty-two 25,000 ℓ/s cryosorption pumps, each connected through a 1.1 m diameter duct to a 0.95 m diameter port in the vacuum chamber wall. To minimize the tritium inventory, the cryosorption pumps will be regenerated, using zirconium-aluminum getter pumps, every four hours to remove the tritium and deuterium that has accumulated on the liquid helium-cooled panels. An additional 32 cryosorption pumps are provided to allow for continued operation during the regeneration period.

Pumping requirements for the neutral beam injectors are very demanding. Twelve injectors will each have gas loads of 110 Torr-ℓ/s during operation. The required pumping speed of $\sim 5 \times 10 \ell$/s will be provided by 100 m^2 of cryosorption panel in each injector. To avoid shutdown during regeneration, an additional 100 m^2 of the panel area must be provided and the design must allow for isolation of that portion of the cryosorption panel to be regenerated.

The principal parameters of the toroidal and neutral beam vacuum systems are shown in Table 9.

The high impedance characteristics of the waveguide used for lower hybrid rf heating will necessitate a separate pumping system to insure adequate vacuum along the length of the waveguide. Each waveguide must have either a mercury diffusion or turbomolecular pump with an effective pumping speed of 10,000 ℓ/s to maintain the required 1×10^{-6} Torr vacuum at the waveguide window.

FIRST WALL

The first wall system consists of a vacuum wall and detachable coolant panels. The free-standing vacuum vessel is constructed from 16 cylindrical segments of 2 cm thick stainless steel plate and is reinforced with an external ring and spar framework. Two circumferential support rings and ten longitudinal spars are on each segment. The 16 segments are joined by formed rings that are welded to the ends of each segment. A chemically bonded Cr_2O_3 coating is applied to the joining surfaces in two of these rings to form a current breaker in the vacuum wall. Detachable 2 cm stainless steel coolant panels are roll-bonded to the inside of the vacuum wall. The surface of the coolant panel facing the plasma is coated with 100-200 microns of beryllium to control impurity contamination of the plasma by stainless steel. The substantial porosity (10-15%) and fine microstructure obtainable with the plasma-spray coating process facilitates gas re-emission, particularly helium, and minimizes blistering erosion. Pressurized water is supplied to the coolant panels by manifolds located in the connecting rings that join the first-wall segments. The toroidal vacuum wall is supported by a three-point per segment, roller/slide pad-type support from the blanket to the lower rings and spars. The three-point support minimizes the size of the reinforcing ring and the roller/slide support minimizes thermal stresses by allowing for expansion of the vessel.

Extensive thermal-hydraulic, mechanical, materials performance, and radiation damage analyses have been performed to evaluate the first-wall performance and to determine the design limits. Results are summarized in Tables 10 and 11.

The stainless steel vacuum wall should maintain its structural integrity for the 10-yr design life under the nominal operating conditions, viz., integrated wall loading of 2.5 MW-yr/m^2, maximum annual neutron fluence of 6×10^{25} n/m^2 (2.8 dpa/yr, 54 appm/yr helium, and 133 appm/yr hydrogen) and maximum wall temperature of $\leq 500°C$. For these conditions the predicted radiation swelling of <4% is tolerable. The limiting criterion is loss of ductility caused by displacement damage and helium generation. For temperatures below 500°C, the residual uniform elongation, which is estimated to be $\geq 1\%$ at the end of the 10-yr life, is considered to be acceptable. The lifetime of the low-Z coating is limited by erosion caused primarily by D-T physical sputtering. A design life of 5 yr for a 100-200 µm thick beryllium coating appears feasible. Only limited data exists with which to estimate the lifetime of the ceramic current breaker; however, bulk radiation effects will likely be the limiting criteria.

In addition to the extensive radiation damage, the coolant panel will be subjected to severe thermal cycling produced by heat deposition on the surface during the plasma burn. Temperature variations in the hottest coolant panel during operation are shown in Fig. 8. The spike is caused by the radiation when Argon is injected to terminate the burn. The strain range for the burn cycle depends on the difference between the maximum and minimum values of ΔT during the
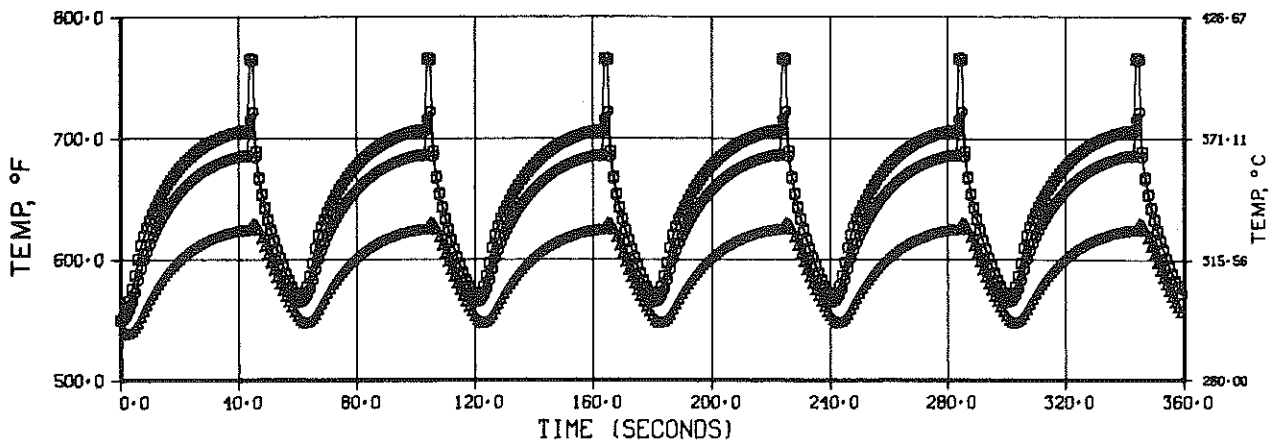
Fig. 8 Transient temperature histories (0.5 MW/m^2). Locations on the coolant exit plane at the surface of the beryllium coating (upper curve), at the surface of the stainless steel in contact with the coating (middle curve), and at the stainless steel surface in contact with the coolant (lower curve).
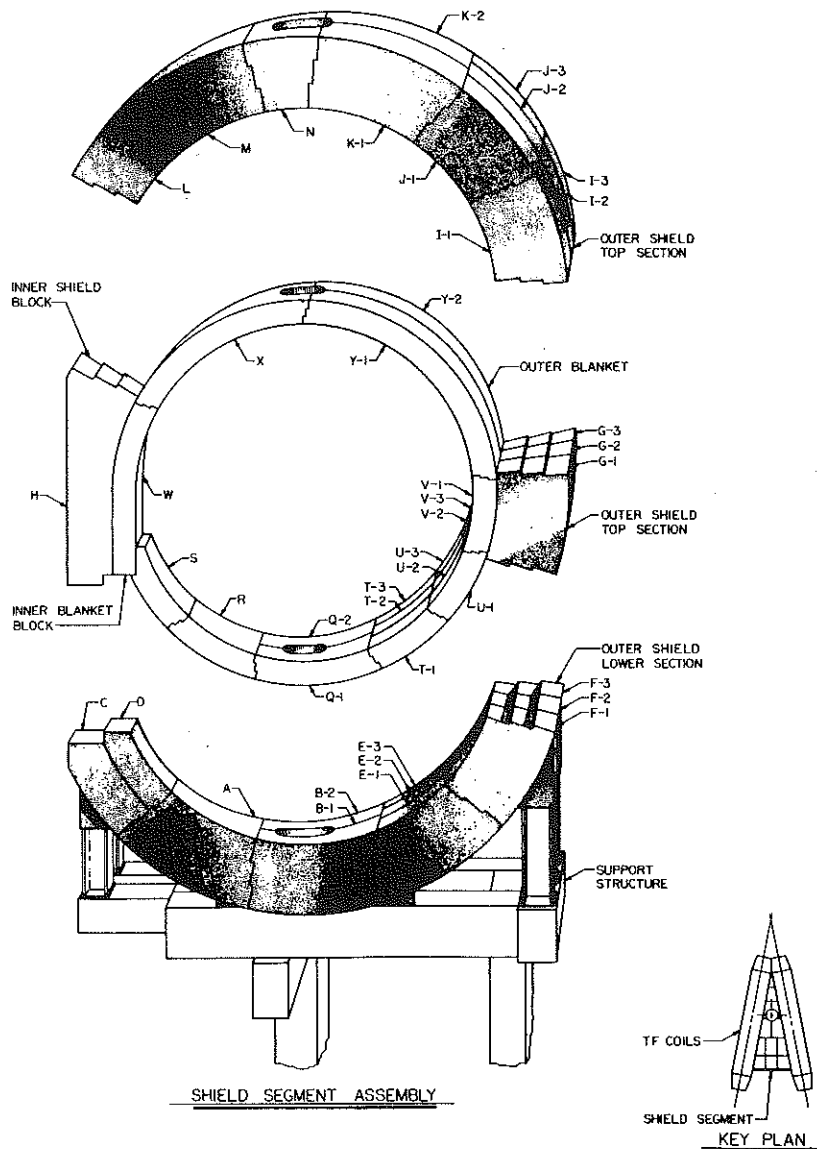

Fig. 9 EPR blanket/shield arrangement

Table 10   First-Wall Operating Parameters

Nominal Operating Conditions

Capacity factor (%)	50
Operating cycle (s)	
Startup	5
Burn	35
Shutdown	5
Exhaust and replenishment	15
Average power loading during burn (MW/m^2)	
Neutron	0.5
Radiation, conduction, convection	0.13

Operating Parameters

Stainless steel vacuum wall	
Maximum temperature (°C)	<500
Minimum yield stress at 500°C (ksi)	17
Maximum annual fluence (n/m^2)	6×10^{25}
Atomic displacement (dpa/yr)	2.8
Helium generation (appm/yr)	54
Hydrogen generation (appm/yr)	133
Stainless steel coolant panel	
Maximum temperature (°C)	380
Minimum yield stress at 500°C (ksi)	17
Maximum annual fluence (n/m^2)	6×10^{25}
Atomic displacement (dpa/yr)	2.8
Helium generation (appm/yr)	54
Hydrogen generation (appm/yr)	133
Maximum heat deposition (W/cm^3)	5.8
Maximum ΔT across panel surface (°C)	20
Maximum ΔT through panel face (°C)	
With Argon shutdown	100
Without Argon shutdown	75
Maximum thermal strain range (%)	
Operating cycle	0.14
Burn cycle	0.09
Beryllium coating	
Maximum surface temperature (°C)	407
Helium generation (appm/y)	780
Hydrogen generation (appm/y)	13
Maximum erosion rate (μm/y)	30
Water coolant	
Maximum pressure (psi)	2000
Velocity (m/s)	1.6
Inlet temperature — first panel (°C)	40
Exit temperature — eighth panel (°C)	310
Pumping power (MW)	<1

Table 11   First-Wall Design Limits[a]

Vacuum Wall

Design life (yr)	10
Integrated neutron wall loading $(MW-yr/m^2)$	2.5
Yield strength — 10 yr (ksi)	75
Uniform elongation — 10 yr (%)	>1
Radiation swelling — 10 yr (%)	<4
Limiting criterion	Ductility

Coolant Panel

Design life (yr)	5
Total burn cycles — 5 yr	10^6
Fatigue lifetime (yr)	5
Radiation lifetime (yr)	8
Limiting criterion	Thermal fatigue

Low-Z Coating

Design life (yr)	3–5
Limiting criterion	D-T sputtering

[a] Based on a neutron wall load of 0.5 MW/m^2 and a plant capacity factor of 50%.

cycle, and the strain range for the plant warmup/cool-down operating cycle is a function of the average ΔT during the burn cycle. Assuming that the duration of the operating cycle is long enough that stress relief occurs, the strain range for the coolant panels with sliding supports is 0.085% for the burn cycle and 0.14% for the warmup/cool-down operating cycle. These values correspond to fatigue design lifetimes for the coolant panels of 5×10^6 burn cycles and 1×10^5 operating cycles. Thus, thermal fatigue will limit the life of the coolant panel to 5 yr, which corresponds to ~10^6 burn cycles, for the current design parameters.

Although the current first-wall system design is based to a large extent on available materials and existing technology, it appears that adequate mechanical integrity of the system can be maintained for suitable reactor lifetimes under the postulated EPR conditions.

BLANKET/SHIELD

The blanket/shield system consists of the blanket, the inner bulk shield, the outer bulk shield, the neutral beam penetration shield, the vacuum duct penetration shield, and the biological shield. In order to insure penetration of the equilibrium field into the plasma region without intolerable distortion or phase delay, the blanket and bulk shield are constructed of 688 electrically insulated blocks, as illustrated in Fig. 9.

The blanket is made up of 0.28 m thick stainless steel blocks, as shown in Fig. 10. Each of the 16 segments of the vacuum chamber is covered by 17 blanket blocks. The blocks are cooled with pressurized water flowing in a network of 1 cm diameter drilled channels, with each block having an independent cooling system.

The bulk shield surrounding each of the sixteen segments of the vacuum wall and blanket consists of 1 inner shield block and 25 outer shield blocks, as shown in Fig. 9. The inner shield block is 0.58 m thick and consists of alternating layers of B_4C and stainless steel disposed so as to maximize the attenuation of neutrons and gamma rays. At the top, bottom, and outside of the torus, the bulk shield is 0.97 m thick and consists (going radially outward) of 0.03 m of stainless steel, 0.15 m of graphite with 1% natural boron, 0.05 m of stainless steel, 0.65 m of lead mortar, and 0.09 m of aluminum. The bulk shield is cooled with H_2O at atomospheric pressure.

Neutral beam lines, vacuum ducts, and other penetrations of the outer blanket and bulk shield represent large (~0.6-1.0 m^2 cross section) streaming paths for neutrons and require special shielding. A special, 0.75 m thick, annular shield surrounds the neutral beam tube after it exits from the bulk shield and extends beyond the TF coils, so that there is no unshielded line-of-sight path from the wall of the beam tube to the TF coils. The inner 0.65 m of this special shield is 50% SS/50% B_4C, followed by 0.05 m of lead and 0.05 m of aluminum.

A pneumatically operated shield plug is closed in the vacuum duct during plasma burn (see Fig. 2). This shield plug consists of two blocks. The inner block is 0.32 m thick, and is fabricated of stainless steel and cooled in the same manner as a blanket block. The outer block is 0.58 m thick, with a material disposition (SS/B_4C) similar to that of the inner shield.

The blanket, shield, and vacuum vessel assembly weighs over 2700 metric tons. This weight is supported from beneath the reactor on 16 individual frames. The frames can move vertically approximately 2 m to facilitate replacement of the blanket and shield blocks. The load is transferred through 32 columns from the reactor foundation to the 16 frames, which in turn support the reactor shielding blocks. The blanket block layer rests on the inner portions of the shield blocks on insulated roller pads to accommodate the high temperature of the blanket and the accompanying thermal expansion. The 350 metric ton vacuum vessel rests on the inner side of the blanket.

Extensive analyses have been performed to evaluate the performance of the blanket/shield system. These analyses are based on a nominal neutron wall load of 0.5 MW/m^2 and a plant capacity factor of 50%. The neutronics effects vary significantly around the wall in the poloidal direction, and a conservative analysis is used. Results are summarized in Table 12.

The 4 cm first wall and the 28 cm blanket region receive $\gtrsim$90% of the neutron and gamma energy. The nuclear heating varies from 3.5 W/cm^2 on the inside to 0.3 W/cm^2 on the outside of the blanket. The radiation damage level in the blanket adjacent to the first wall is ~1.7 dpa/yr and drops by a factor of 2 every ~7 cm going through the blanket. Operating temperatures in the load bearing portions of the blanket are, like the first-wall temperatures, restricted to $\leq$500°C, but may be allowed to rise above this level in nonstructural components. After 10 yr at a wall loading of 0.5 MW/m^2 and a 50% capacity factor, the swelling in the blanket adjacent to the first wall is expected to remain below 2%, the uniform elongation will drop to ~3%, and the yield strength will increase to ~75 ksi. As the neutron radiation is attenuated through the blanket, the swelling will be reduced to zero after a few cm, and the tensile properties will approach those of unirradiated material (~22% uniform elongation and ~20 ksi yield strength). The effect of creep and fatigue will be less than in the first wall since the blanket is not exposed to the surface radiation from the plasma and will not undergo the large thermal cycling of the first wall. Helium production rates will still be high in the first few cm, but the temperature limit of 500°C should insure against helium embrittlement which is observed at temperatures above 550°C.

Regions in the outer bulk shield, 20 cm thick, surrounding the neutral beam penetrations will be constructed and cooled similar to the blanket. The remainder of the bulk shield will receive ~7% of the radiation energy. The major effect of radiation on boron carbide is the buildup of helium from (n,α) reactions which can induce swelling and cracking if it is present in high concentrations. Neutron irradiation can also substantially reduce the thermal and electrical conductivity. The degree to which radiation affects the bulk properties depends to a large extent on the amount of porosity present in the unirradiated material. The first layer of boron carbide in the inner shield will be the most seriously affected by the neutron irradiation. The first few cm of boron carbide will produce ~3500 appm of helium during a 10 yr lifetime, but helium production will fall off rapidly past this point. This amount of helium is not expected to induce significant swelling or cracking if a sufficient porosity exists to accommodate the gas. Helium escaping from the boron carbide must be vented to prevent buildup of gas pressure within the shield. For the conditions expected in the
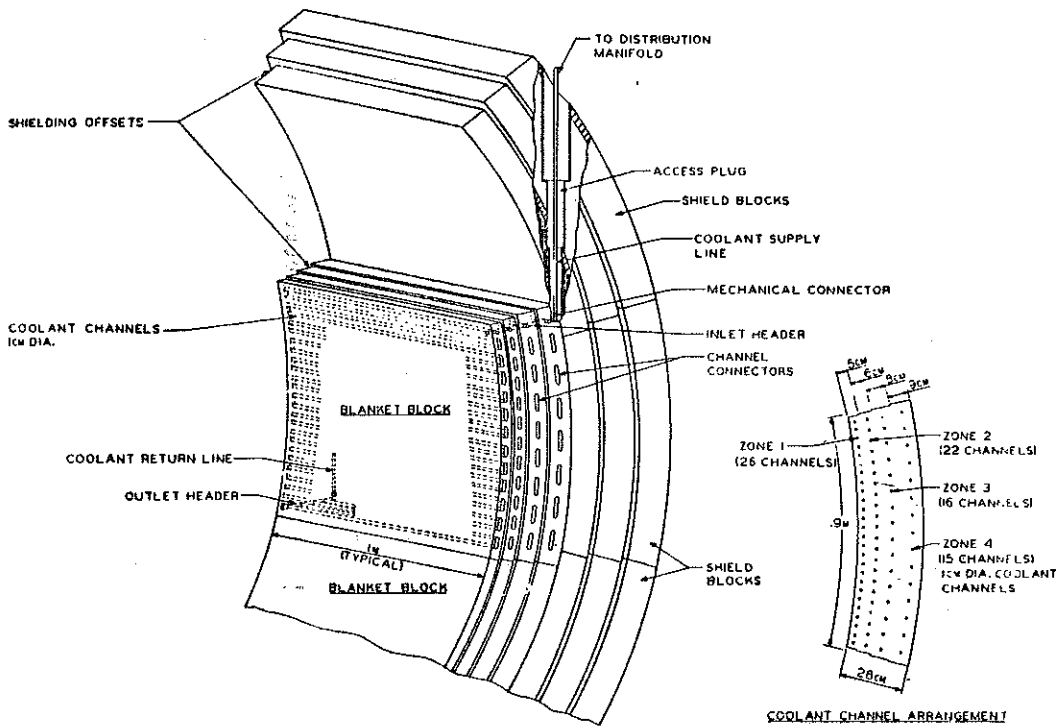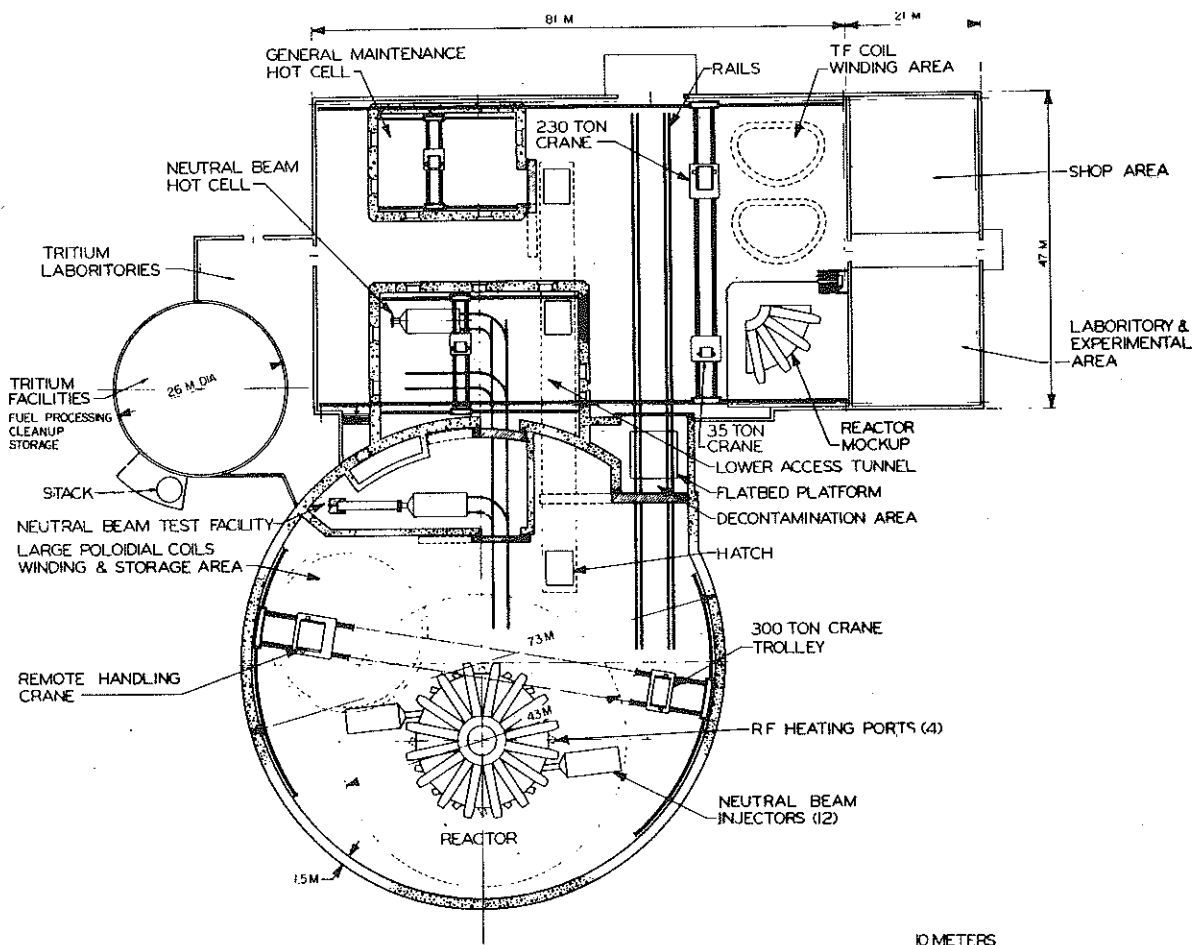
Fig. 10   Blanket block

Fig. 11   Reactor containment building

Table 12   Summary of Blanket Design Parameters

Design basis operating life (yr)	10
Nominal power during burn (MW)	400
Design basis neutron wall loading (MW/m^2)	0.5
Plant capacity factor (%)	50
Blanket structure	
Thickness (m)	0.28
Type metal/volume fraction	316-SS/0.9
Type coolant/volume fraction	$H_2O/\leq 0.05$
Penetration volume fraction	
Inner blanket	∿0.02
Outer blanket	∿0.05
Maximum temperatures (°C)	
In support structures	500
In bulk materials	550
Nuclear parameters	
Maximum heat deposition (W/cm^3)	3.5
Maximum fluence at 2.5 MW-yr/m^2 (n/m^2)	5×10^{26}
Maximum dpa at 2.5 MW-yr/m^2 (dpa)	17
Maximum helium production at 2.5 MW-yr/m^2 (appm)	230
Maximum hydrogen production at 2.5 MW-yr/m^2 (appm)	600
Mechanical parameters	
Design stress in support structure (ksi)	≤ 10
Minimum material yield stress (ksi)	20
Ductility at 2.5 MW-yr/m^2 (% uniform elongation)	> 3
Swelling at 2.5 MW-yr/m^2 (% of initial volume)	≤ 2
Maximum torque from pulsed fields (ft-lb)	125,000
Coolant parameters	
Type	H_2O
Maximum pressure (psig)	2000
Pressure drop (psig)	<15
Maximum velocity (m/s)	2.4
Pumping power (MW)	<1
Coolant inlet temperature (°C)	40
Maximum coolant exit temperature (°C)	309
Residual activity from first-wall/blanket/shield after 2 yr operation in Ci/MWt	
Immediately after shutdown	3.5×10^6
1 yr after removal	8.0×10^5
10 yr after removal	7.0×10^4
100 yr after removal	60

EPR, the graphite in the outer bulk shield will densify rather than swell. It is expected that the volume change of graphite due to irradiation can be minimized by a suitable choice of material and should not present a problem. Helium production in the first few cm of the graphite/1% boron will reach ~770 appm after a 10 yr lifetime. As with boron carbide, porosity and venting considerations must be factored into the shield design to accommodate the helium. The materials lying past the first layer of boron carbide in the inner shield and the graphite in the outer shield receive a relatively small neutron fluence, and the bulk properties should not be adversely affected. The lead mortar and aluminum in the outer shield will operate at temperatures below 100°C, which is well below the ~150°C at which the lead mortar will begin to break down.

ACCESS AND MAINTENANCE

During operation, the biological dose in regions external to the TF coils is about 10^6 mrem/hr, which is too high to permit access to the inside of the reactor building for any reasonable length of time. Outside the 1.5 m thick concrete building wall, the dose is about 1 mrem/hr. The biological dose in the vacuum chamber inside the first wall is 6×10^9 mrem/hr at shutdown and after 1 yr of cooldown the dose is 1×10^9 mrem/hr. After one day of cooling, the dose is 600 mrem/hr at a position above the reactor at the location of the TF coils and 2 mrem/hr outside the TF coils. The latter result does not include the effect of penetration streaming or activation of the neutral beam injector. These calculations indicate that the dose rate is too high to permit unshielded personnel access to the reactor during operation. At best, limited access would be allowed within a few days of shutdown. Personnel exposure can be reduced by two orders of magnitude by 10 cm of lead shielding.

The general approach to maintenance for the EPR is by use of remote handling apparatus. All large components will be repaired in place, where possible. This includes the vacuum vessel and the lower EF and OH coils. Smaller components like the blanket and shield blocks will be repaired in the hot cells. Special in-vessel remotely operated equipment will be designed to repair, replace, and inspect any portions of the vacuum vessel or first-wall panels that have been damaged. Support facilities for remote operations include a remotely-operated overhead crane/ manipulator with a shielded personnel cab, floor-mounted snorkel-type units for servicing the vertical portions of the reactor and basement-positioned apparatus for maintaining the lower components of the reactor. A full-scale, quarter section mockup of the reactor is vital to all remote operations.

TRITIUM

The EPR tritium handling system must separate tritium and deuterium from the spent fuel and must be capable of building atmosphere cleanup in the event of a large tritium release. The key tritium facility operating parameters are given in Table 13. The principal assumptions applied in determining these parameters are: (1) that the throughput/burnup ratio will be approximately 50; (2) that the fuel cycle turnaround time (fuel holdup) time will be 4 hr or less; and (3) that the initial tritium inventory of ≤ 1.5 kG will be supplemented as needed (from an outside production facility) to match the burnup encountered during operation. The fuel cycle turnaround time is

determined mainly by the regeneration cycle on the cryosorption pumping system for the toroidal plasma chamber. The present plan is to carry out this regeneration cycle on a 4-hr basis.

Calculations have been made to estimate the rate of tritium permeation from the plasma chamber into the first-wall cooling water circuit. These calculations show that the tritium level in the first-wall cooling water ($\sim 10^5$ ℓ) increases to a maximum of ~ 1 Ci/ℓ. The handling practices associated with this pressurized cooling water would essentially be the same as those currently applied in the pressurized D_2O primary circuits of heavy water reactors that commonly run up to 10 Ci/ℓ.

Potential off-site tritium exposure calculations have been made. Two events leading to off-site exposure due to the release of tritium have been considered. The first event considers 2% ($\sim 4 \times 10^5$ Ci) of a total inventory of 2 kg of tritium released at ground level as water vapor in an accident. The dose commitment for an individual at the site boundary is 23.5 rem (whole body) at 500 m and 7.4 rem (whole body) at 1000 m as compared to the 10 CFR 100 guideline for total body dose in an accident of 25 rem. The second event is the continuous daily release of 100 Ci of tritium, for which the concentration at 500 m is $\sim 5 \times 10^{-9}$ Ci/m^3 and at 1000 m is $\sim 2 \times 10^{-9}$ Ci/m^3. ERDA Manual 0524 gives the uncontrolled concentrations guide as 2×10^{-7} Cu/m^3.

FACILITY DESCRIPTION

The reactor complex consists of 11 major facilities covering an area of 65,000 m^2. The focal point is the reactor containment building (Fig. 11), a structure 73.2 m in diameter $\times$ 50 m high made of reinforced concrete, 1.5 m thick, to meet both structural and biological requirements. A thin steel membrane, 1 cm thick, lines the inside walls of the building, forming a barrier in the event of a tritium release. The seal is carried through all penetrations and access ways. A reactor pedestal is provided slightly offset from the center of the building for convenience in positioning the 300 ton overhead polar crane used in assembly and maintenance of the reactor. The building is equipped for remote maintenance of the reactor.

COSTS AND SCHEDULES

The estimated total direct capital cost for the EPR is $579 M. Adding 25% for engineering and 25% for contingency brings the grand total to $868 M. A cost breakdown is given in Table 14.

A detailed design and construction schedule has been developed. Eight years are required from the initiation of preliminary design to initial operation, and six years are required from the initiation of detailed Title II engineering design to initial operation of EPR. This schedule is based on two-shift/ five-days-a-week operation.

REFERENCE

1 Stacey, W. M., Jr., et al, "Tokamak Experimental Power Reactor Conceptual Design," ANL/CTR-76-3, Argonne National Laboratory (1976).

Table 13 Summary of Tritium-Handling Facility Parameters

	B_{max}^{TFC}	
	8 T	10 T
General		
Power during burn (MW)	200	500
Burn cycle duty cycle (%)	75	75
Plant availability factor (%)	67	67
Tritium burnup (g/day)	26	64
Throughput/burnup ratio	50	50
Tritium delivery rate (g/hr)	60	150
Fuel cycle turnaround time (hr)	4	4
Plant inventory (kg)	0.6	1.5
Annual tritium consumption at 50% capacity factor (kg)	6.4	16
Tritium Inventory Disposition		
Cryosorption pumps (g)	240^{a}	600^{a}
Getter beds (g)	240^{a}	600^{a}
Distillation columns (g)	10^{a}	25^{a}
Fuel cycle hardware (g)	10^{a}	25^{a}
Storage (g)	$\sim 500^{a}$	$\sim 1300^{a}$
Anticipated mean inventory (g)	600	1500
Fuel Cycle		
Nature of fuel processing and recycle systems	Nonmetallic element removal Debris removal Isotopic enrichment Fuel storage Fuel delivery	
Type of mainstream enrichment	Cryogenic distillation	
No. of columns	6	
No. of equilibrators	1	

^{a}Maximum value at any single time.

Table 14 Plant Capital Investment Direct Cost Estimate

	M^{a}
Structures and site facilities	67.3
Reactor	248.6
Reactor plant facilities	245.0
Auxiliaries	18.0
TOTAL	578.9
Engineering (25%)	144.7
Contingency (25%)	144.7
GRAND TOTAL	868.3

^{a}FY 1976 dollars.